

Predicting stability of a prototype un-bonded fibre-reinforced elastomeric isolator by finite element analysis

†Thuyet Van Ngo¹, *Anjan Dutta², and Sajal K. Deb²

¹PhD student, Department of Civil Engineering, IIT Guwahati-781039, Assam, India.

²Professor of Civil Engineering Department, IIT Guwahati-781039, Assam, India.

*Presenting author: adutta@iitg.ernet.in

†Corresponding author: ngothuyetxd@gmail.com

Abstract

Fibre-reinforced elastomeric isolator (FREI) in an un-bonded application is an improved device for seismic mitigation of low-rise buildings. It is expected to reduce the cost, weight and provide easier installation in comparison to the conventional elastomeric isolator, which consists of elastomeric layers interleaved with steel plate as reinforcement. The horizontal response of un-bonded isolator is nonlinear due to rollover deformation and the horizontal stiffness is a function of both vertical load and horizontal displacement. Most previous studies have been focused to develop the model for predicting stability of the bonded conventional elastomeric isolators with low shape factors. In the present study, predicting stability of a prototype un-bonded FREI is presented based on the dynamic response utilizing finite element (FE) analysis. A prototype isolator is investigated under the variation of vertical loads and cyclic horizontal displacement to evaluate the performance and the effect of the vertical load on the behaviour of the isolator. FE analysis result shows that the critical load capacity of the isolator is significantly higher than the design vertical load, and the effective horizontal stiffness decreases with the increase in the vertical loads. Furthermore, the horizontal response of the isolator is also conducted under the design vertical load and increasing horizontal displacement up to $2.00t_r$ to observe the rollout instability.

Keywords: Fibre reinforced elastomeric isolator, un-bonded isolator, rollout instability, dynamic stability, buckling, critical load, analytical model.

Introduction

Seismic isolation is a well-known earthquake mitigation technique, where a layer of low horizontal stiffness is introduced between the foundation and superstructure. As a result, the natural period of vibration of the structure changes beyond the high-energy period range of earthquakes, and hence the seismic energy transferred to the structure is significantly reduced. Conventional steel reinforced elastomeric isolators (SREIs) have become a widely accepted technique in the structure over the past four decades for protecting the buildings from strong ground motion. They consist of alternating layers of rubber bonded to intermediate steel shims with two steel end plates at top and bottom. In general, SREIs are often applied for large, important buildings like hospitals and emergency centres, in countries such as Japan, New Zealand, United States, Mexico, Italy, etc. This limited use is largely due to the high material, manufacturing and installation costs. It is expected that the use of seismic isolators can be extended to ordinary low-rise housing if the weight and cost of the isolators are reduced. In view of this, fibre reinforced elastomeric isolators (FREIs) are proposed by replacing steel shims in conventional isolators by multi-layer of fibre fabric as reinforcement sheets to reduce their weight and cost. An un-bonded fibre reinforced elastomeric isolator (U-FREI) is a significant effort to improve FREI by removing two steel end plates and installing directly between the foundation and superstructure without any connection to these boundaries. Using U-FREI would reduce the weight and cost, easier installation, and can be made as a long strip and then easily cut to the required size. It means that the U-FREIs can be used for low-rise buildings subjected to earthquake loading in the developing countries.

The stability of elastomeric isolators is an important parameter for the design of seismic isolation systems. Elastomeric isolators are used in the structure to resist strong ground motion of earthquake with large displacement. Study on stability of elastomeric isolators refers to the determination of critical load carrying capacity while undergoing large horizontal

displacement. Generally, the critical load carrying capacity of isolator reduces with increasing horizontal displacement due to the reduction of the effective horizontal stiffness. The critical load in an elastomeric isolator is defined as the vertical load for which the horizontal stiffness is reduced to zero.

Procedures to evaluate critical loads of elastomeric isolators are based on an extension of Euler buckling load theory by Southwell [1932] to experimentally determine the buckling load in the flexible columns and a theoretical approach by Haringx [1948, 1949(a,b)] to predict the stability of rubber rods. Later, Buckle and Kelly [1986] carried out experimental studies to evaluate stability of SREIs under quasi-static loading using Southwell's procedure and under dynamic loading on a scaled model of bridge deck using shaking table test. Stable rollover of isolators could be observed in this study. These studies were however conducted with linear model and under small imposed displacement. In general, the behaviour of elastomeric isolators is nonlinear when subjected to large horizontal displacement under strong ground motion.

Some extensive analytical and numerical studies were performed to analyze the stability limit in elastomeric isolators and model their behaviour. Koh and Kelly [1989] proposed a two-spring mechanical model and visco-elastic stability model based on extension of Haringx's theory. The influence of vertical load on the horizontal stiffness of SREIs was evaluated. Stanton, et al. [1990] studied the stability of steel laminated elastomeric bearings using a modified linear model from Haringx's theory with configuration accounting for nonlinearity. When an elastomeric bearing was simultaneously subjected to vertical load and increasing lateral displacement, the shear force on bearing was observed to have passed through a maximum value. This point is the location of zero tangential stiffness, which is considered as the stability limit. Buckle and Liu [1993, 1994] experimentally determined the critical buckling behaviour of SREIs at high shear strains and proposed a simple reduced-area formula to estimate the critical load in bearings by overlapping area method. However, this method predicted a simple linear (for rectangular bearings) or nearly linear (for circular bearings) reduction in critical load with lateral displacement independent of material or geometric parameters of bearings. Actually, this reduction is not linear as observed in experimental tests. A nonlinear analytical model consisting of two-spring systems was proposed by Nagarajaiah and Ferrell [1999] in an effort to more accurately predict the critical load capacity of SREIs of different sizes and shape factors at a certain lateral displacement. The model was developed from two-spring model by Koh and Kelly with large displacement, large rotations and nonlinearities in shear and rotational stiffness of the bearing. The model was shown to predict a reduction in the critical load capacity with increasing lateral displacement, and the critical load capacity was not equal to zero at a lateral displacement equal to width of bearing. Buckle, et al. [2002] validated the nonlinear analytical solutions proposed by Nagarajaiah and Ferrell [1999] and determined the effect of lateral displacement on critical load by experimental tests with a series of low-shape-factor elastomeric bearings. Iizuka [2000] proposed a macroscopic model based on the two-spring model by Koh and Kelly, where the linear springs were replaced by nonlinear springs for predicting the stability of laminated rubber bearings at large deformations and under different vertical loads. The nonlinear parameters of the shear and rotational springs were determined from basic load test. Detailed nonlinear finite element analysis and an improved analytical formulation for predicting the reduced load-carrying capacity of bearings based on overlapping area method were also presented by Weisman and Warn [2012]. A recent study by Sanchez, et al. [2013] focused on experimental tests to examine the behaviour of steel reinforced elastomeric bearings at and beyond their stability limits. Three methods (two quasi-static tests and one dynamic loading test) were conducted to predict the stability limits of bearings and compared with the reduced-area formulation. Han, et al. [2013] proposed a modified analytical model based on the sensitivity analysis using Iizuka's model for the prediction of critical load capacity of bearings. Vemuru, et al. [2014] presented an enhanced analytical model based on a nonlinear analytical model by Nagarajaiah and Ferrell for application beyond stability limit. Thus, most previous studies were focused to improve the analytical model for predicting stability of elastomeric isolators and these models were developed for bonded conventional elastomeric isolators. Therefore, it is necessary to study on the stability of FREIs in unbonded application.

As a result of un-bonded application, isolators undergo large deformation due to stable rollover under large horizontal displacements. Some regions of the top and bottom surfaces of isolator lose contact with the superstructure and substructure when the isolator is displaced horizontally. The reduction of the effective horizontal stiffness due to rollover deformation increases the seismic mitigation efficiency of isolator; but stability of isolator must be maintained. If an un-bonded FREI with a certain shape factor, S (defined as the ratio of the loaded area to load free area of a rubber layer) and aspect ratio, R (as the ratio of width to total height of the isolator) is able to achieve positive incremental load-resisting capacity during the course of cyclic loading, the isolator is assumed to be stable. On the other hand, the effective stiffness of an un-bonded isolator may also increase due to the initiation of contact between the vertical faces of the elastomer layers with the support surfaces, when they undergo very large displacement. Thus, a transition region between the decrease and increase in the effective stiffness is observed, and at certain value of displacement within this region, the increase in the effective stiffness of isolator due to contact exceeds the decrease in the stiffness due to rollover, and a hardening behaviour is occurred. This hardening behaviour observed in an un-bonded FREI is considered to be an advantageous characteristic since it can limit the maximum horizontal displacement of the isolation system in situations beyond the design basis seismic events. Studies related to the prediction of stability of un-bonded FREIs under cyclic loading were carried out experimentally by Raaf, et al. [2011]. In this study, authors proposed a method of fitting a polynomial to experimental force-displacement hysteresis data to predict the critical load capacity of isolator. This method was used to determine the fitted backbone curve and horizontal tangential stiffness. Additional studies for the buckling behaviour of un-bonded isolators were conducted using theoretical analysis by Kelly, et al. [2011, 2012].

From the above-mentioned literature review, it is observed that most of the models for predicting stability of elastomeric isolators are developed for conventional isolators in bonded application. There are very few studies for ascertaining the stability of FREIs in an un-bonded application. In addition, scaled sizes of elastomeric isolators were considered in these studies with low shape factors and aspect ratio, e.g. Nagarajaiah and Ferrell [1999], Buckle, et al. [2002] considered isolators with $S = 1.67$ to 10 ; Sanchez, et al. [2013] with $S = 5.51$ to 10.16 ; Han, et al. [2013] with $S = 5$ to 10.2 ; Vemuru, et al. [2014] with $S = 10.64$. Experimental studies were conducted for isolators with larger shape factors such as Raaf, et al. [2011] with $S = 11$ but for a scaled size of $70 \times 70 \times 24$ mm; Weisman and Warn [2012] with $S = 10$ to 12 . Therefore, it is necessary to carry out the studies for predicting the stability of a prototype U-FREI with high shape factor.

This paper presents studies related to predicting stability of prototype un-bonded FREI by FE analysis. Determination of the stability limit of an prototype isolator by experimental tests is relatively accurate, but it is difficult to investigate in laboratory due to constraints of experimental facility. In this study, predicting stability of a prototype un-bonded isolator is investigated by FE analysis and the accuracy of the response of the isolator under design vertical load and increasing horizontal displacement up to $0.89t_r$ (80 mm) is validated by comparing with the experimental results. A prototype FREI with size of $250 \times 250 \times 100$ mm, shape factor of 12.5 and aspect ratio of 2.50 is investigated under the variation of vertical load and cyclic horizontal displacement to determine the critical load capacity and the effect of the vertical load on the behaviour of this isolator. Further, the horizontal response of the un-bonded isolator is also evaluated under the design vertical load and increasing horizontal displacement up to $2.00t_r$ (180 mm) to observe the rollout instability of the isolator.

Procedure for determination the critical load capacity of un-bonded FREI

As observed from literature survey, stability of an elastomeric isolator is evaluated based on the relation of shear force with horizontal displacement. The critical load capacity of the elastomeric isolator is defined as the vertical load for which the horizontal stiffness is reduced to zero (or zero tangential stiffness). When the elastomeric isolator is subjected to simultaneously the vertical load, P , and increasing horizontal displacement, u , shear force may pass through a maximum value, as illustrated in Fig. 1. The point of maximum shear force is considered the stability limit defined by the critical horizontal displacement, u_{cr} , and corresponding vertical load referred to herein as the critical load, P_{cr} .

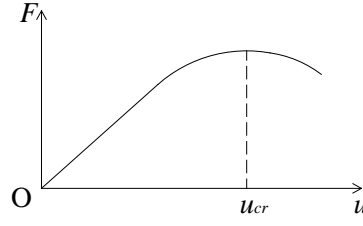


Fig. 1. Shear force versus horizontal displacement

From theoretical analysis, the critical load is defined as the point, where the shear force reaches a maximum value:

$$K_h = \frac{\partial F}{\partial u} = 0 \quad (1)$$

Using chain rule,

$$K_h = \frac{\partial F}{\partial u} = \frac{\partial F}{\partial P} \times \frac{\partial P}{\partial u} = 0 \quad (2)$$

where F , u , P are shear force, horizontal displacement and vertical load, respectively. There is no requirement that $\partial F / \partial P$ must be equal to zero. Therefore,

$$\frac{\partial P}{\partial u} = 0 \quad (3)$$

where $\partial P / \partial u$ = derivative of the vertical load with respect to the horizontal displacement.

For a conventional elastomeric isolator in bonded application, the prediction of critical load capacity is often conducted by two quasi-static methods. In the first method, the isolator is subjected to a constant vertical load, P , and a monotonically increasing horizontal displacement, u , until the isolator reaches its stability limit ($K_h = 0$). The point of equilibrium is determined directly from shear force-horizontal displacement response as the point where the slope equals zero. The second method includes shearing the isolator to a constant horizontal displacement, u and applying monotonically increasing vertical load, P , while monitoring a reduction in shear force F . Repeating this procedure for different horizontal displacement levels provides unique equilibrium trajectories (F vs P) from which the point of neutral equilibrium, thus critical point (u_{cr} , P_{cr}) can be indirectly obtained.

However, for a FREI in un-bonded application subjected simultaneously to vertical load and horizontal dynamic displacements, the evaluation of critical load needs to be appropriately considered. Particularly for performance-based design, it is important to extend the theoretical understanding on the stability of isolators based on static/quasi-static methods to dynamic behaviour and enhance the ability to predict their response when subjected to extreme earthquake loading. Thus, it should use a dynamic method under cyclic loading to evaluate the critical load capacity of isolator in an un-bonded application.

In dynamic method, the un-bonded isolators undergo simultaneously a variation of the vertical load and cyclic horizontal displacement. Two important parameters such as the effective horizontal stiffness and damping factor are obtained from the hysteresis loops. The effective horizontal stiffness of isolator at a amplitude of horizontal displacement is defined as

$$K_{eff}^h = \frac{F_{max} - F_{min}}{u_{max} - u_{min}} \quad (4)$$

where, F_{max} , F_{min} are maximum and minimum value of the shear force,
 u_{max} , u_{min} are maximum and minimum value of the horizontal displacement.

The equivalent viscous damping of isolator (damping factor, β) is computed by measuring the energy dissipated in each cycle (W_d), which is the area enclosed by the hysteresis loop. The formula to computed β is given by

$$\beta = \frac{W_d}{2\pi K_{eff}^h \Delta_{max}^2} \quad (5)$$

where Δ_{max} is the average of the positive and negative maximum displacements.

Horizontal stiffness of an un-bonded FREI has two components, namely, horizontal secant stiffness and tangential stiffness. The present study is intended to determine the critical load at which the tangential stiffness becomes zero. In order to calculate the critical buckling load from the hysteresis loops obtained from the dynamic method, a curve is fitted to shear force-displacement hysteresis. According to the previous studies by Toopchi-Nezhad, et al. [2008] and Raaf, et al. [2011], a method of fitting a polynomial to shear force-displacement hysteresis data is developed. The fitted curve, denoted as backbone curve, represents an idealized evaluate of horizontal response of an un-bonded FREI with the damping forces removed (Fig. 2).

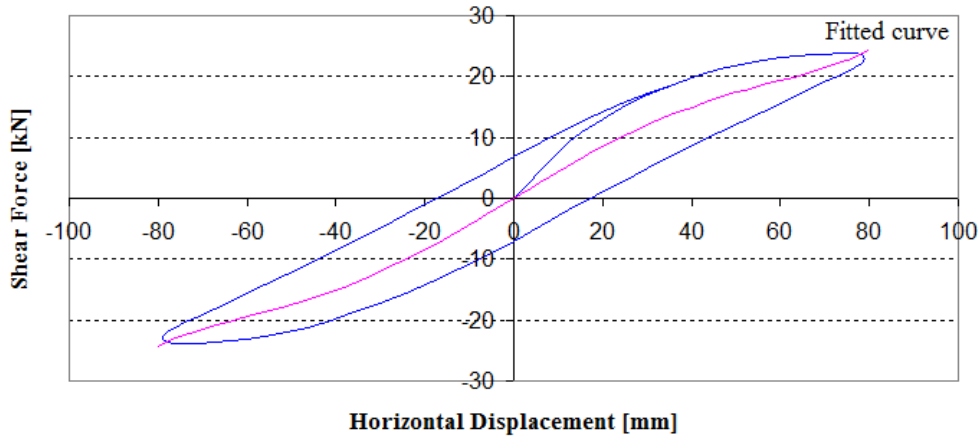


Fig. 2. Illustration of a fitted backbone curve in a hysteresis loop

The total horizontal load, $f_{b,i}$, experienced by the i^{th} isolator is described as:

$$f_{b,i}(t) = f_{sb,i}(t) + f_{db,i}(t) \quad (6)$$

where, $f_{sb,i}$ is stiffness force and $f_{db,i}$ is the corresponding force due to damping.

In a simple approach, the stiffness force can be modelled as a polynomial of order 5 given by:

$$f_{sb,i}(t) = k_{b,i}(v_b(t)) \times v_b(t) = [b_0 + b_1 v_b(t) + b_2 v_b^2(t) + b_3 v_b^3(t) + b_4 v_b^4(t)] \times v_b(t) \quad (7)$$

$$f_{sb,i}(t) = b_0 v_b(t) + b_1 v_b^2(t) + b_2 v_b^3(t) + b_3 v_b^4(t) + b_4 v_b^5(t)$$

where, $v_b(t)$ is horizontal displacement and $k_{b,i}(v_b(t))$ is the horizontal secant stiffness as a function of horizontal displacement:

$$k_{b,i}(v_b(t)) = b_0 + b_1 v_b(t) + b_2 v_b^2(t) + b_3 v_b^3(t) + b_4 v_b^4(t) \quad (8)$$

The five parameters b_0 to b_4 are determined by applying a least squares fit to shear force-displacement hysteresis data.

The corresponding force due to damping, $f_{db,i}$ represents an idealized Rayleigh damping:

$$f_{db,i}(t) = c_{b,i}(t) \times \dot{v}_b(t) \quad (9)$$

where $c_{b,i}(t)$ is damping coefficient dependent on a equivalent viscous damping ratio ξ , tributary mass of structure on each isolator (m_i) and the horizontal secant stiffness $k_{b,i}(v_b(t))$:

$$c_{b,i}(t) = 2\xi\sqrt{k_{b,i}(v_b(t))m_i} \quad (10)$$

The tangential stiffness of the i^{th} isolator, $k_{tb,i}(v_b(t))$, as a function of horizontal displacement is

$$k_{tb,i}(v_b(t)) = \frac{df_{sb,i}(t)}{dv_b(t)} = b_0 + 2b_1v_b(t) + 3b_2v_b^2(t) + 4b_3v_b^3(t) + 5b_4v_b^4(t) \quad (11)$$

where the parameter b_0 is the tangential stiffness of the i^{th} isolator at $v_b(t)=0$.

According to the remark of the previous study by Stanton, et al. [1990], the tangential stiffness at zero horizontal displacement in a shear force-displacement hysteresis is referred to as the transverse stiffness (K_t) of the isolator. The transverse stiffness is not necessarily the minimum tangential stiffness in every fully reserved hysteresis loop under constant vertical load. However, the transverse stiffness represents the tangential stiffness at which zero horizontal stiffness first occurs under increasing vertical load. The vertical load corresponding to a transverse stiffness of zero ($K_t = 0$) is defined as the critical buckling load under cyclic loading for an un-bonded FREI.

Prototype un-bonded fibre-reinforced elastomeric isolator

Prototype FREI considered in this study were manufactured by METCO Pvt. Ltd., Kolkata, India. These are already in use in an actual building in Tawang, India. Figure 3 shows the view of a typical prototype isolator with component layers and finite element model. The isolator comprises of 17 layers of fibre reinforcement sheets interleaved and bonded between 18 layers of rubber. Natural rubber and bi-directional ($0^0/90^0$) carbon fibre fabric are used in the isolator with the thickness of 5.0 and 0.55 mm for each layer of rubber and fibre, respectively. The physical dimensions and material properties of the isolator are shown in Table 1.

Finite element modelling

In this paper, fibre reinforced elastomeric isolator is numerically simulated using FE method in Ansys (v.14). The isolator is subjected to a variation of the vertical load and cyclic horizontal displacement to predict the stability of the isolator in an un-bonded application. FE analysis can address many issues which are rather difficult in closed-form solution. Analysis of isolator using FE method has some prominent advantages for the description of the detailed stress and strain of layers. Further, FE analysis can easily evaluate the response of the prototype isolator under high vertical load and large horizontal displacement, which is very difficult experimentally due to limitation of capacity in experimental facility.

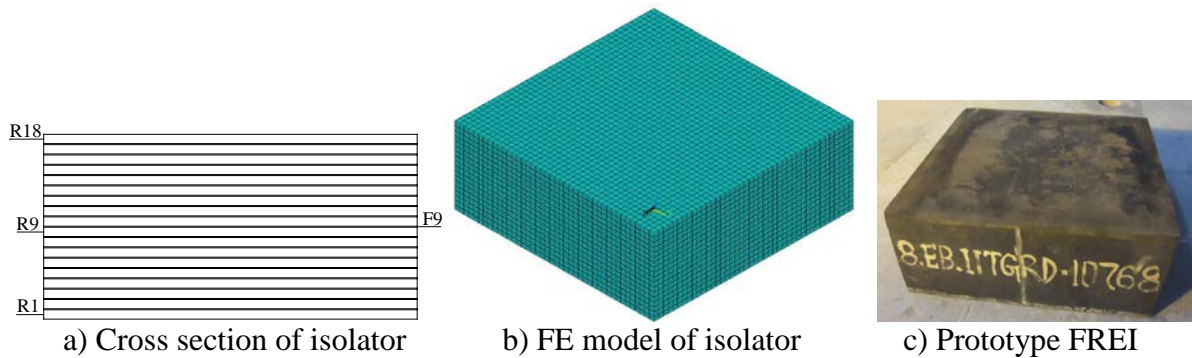


Fig. 3. The component of isolator

Table 1. Geometrical details and material properties of the square isolator

Description	Values
Size of specimen, <i>mm</i>	250x250x100
Number of rubber layer, (n_e)	18
Thickness of single rubber layer, (t_e), <i>mm</i>	5
Total height of rubber, (t_r), <i>mm</i>	90
Number of fibre layer, n_f	17
Thickness of single fibre layer, (t_f), <i>mm</i>	0.55
Shape factor, (S)	12.5
Aspect ratio, (R)	2.50
Initial shear modulus of elastomer, (G_o), <i>MPa</i>	0.90
Elastic modulus of carbon fibre reinforcement, (E_f), <i>GPa</i>	40
Poisson's ratio of carbon fibre reinforcement, (ν_f)	0.2

General description of the model

In this study, the isolator is modelled by elements having capabilities like large strain, incompressibility of material and nonlinear solution convergence. Incompressible material may lead to some difficulties in numerical simulation, such as volumetric locking, inaccuracy of solution, checkerboard pattern of stress distributions, or occasionally, divergence. Lagrange multiplier-based mixed u - P element is used to overcome incompressible material problems. These elements are designed to model material behaviour with high incompressibility such as fully or nearly incompressible hyper-elastic materials and nearly incompressible elasto-plastic materials (high Poisson's ratio or undergoing large plastic strain). Lagrange multipliers extend the internal virtual work so that the volume constraint is included explicitly. Further, an updated Lagrangian approach has been used in this study to update the local coordinate system on the deformed configuration of element when the isolator is subjected to very large horizontal displacement.

In the FE model of FREI, the elastomer is natural rubber which exhibits nonlinear behaviour. It is modelled using SOLID185 which is an eight-node structural solid element having three degrees of freedom at each node such as translations in the nodal x, y, and z directions. The fibre reinforcement is modelled using SOLID46 which is a 3-D eight-node layered structural solid designed to model layered thick shells or solid. Fibre-reinforcements are provided in the form of bi-directional ($0^0/90^0$) layers and bonded between rubber layers. Two rigid horizontal plates are considered at the top and bottom of the isolator to represent the superstructure and foundation. Vertical load and horizontal displacement are applied at the top plate which is allowed to move both in the vertical and horizontal directions, while all degrees of freedom of bottom plate are constrained. In order to study un-bonded FREI, surface-to-surface contact elements are used. Contact element CONTA173 is used to define the exterior rubber surfaces and target element TARGE170 is used to define the interior surface of top and bottom rigid plates. The contact element supports the Coulomb friction model to transfer the shear forces at the interface of contact and target surface. The model is meshed using hexagonal volume sweep.

Material models used for the rubber and fibre reinforcement

Material properties of isolator shown in Table 1 are used in FE model. Elastomer is modelled with hyper-elastic and visco-elastic parameters. Hyper-elasticity refers to materials which can experience large elastic strain that is recoverable. Rubber-like and many other polymer materials fall in this category. The constitutive behaviours of hyper-elastic materials are usually derived from the strain energy potentials. Further, hyper-elastic materials generally have very small compressibility. This is often referred to as incompressibility. Hyper-elastic materials have a stiffness that varies with the stress level.

In this study, Ogden 3-terms model has been adopted to model the hyper-elastic behaviour of the rubber which is characterized by shear (G_e) and bulk (k_e) modulus of the rubber and the visco-elastic behaviour is modelled by Prony Visco-elastic Shear Response parameter. The material parameters used are [Holzapfel, 1996].

Ogden (3-terms): $\mu_1 = 1.89 \times 10^6$; $\mu_2 = 3600$; $\mu_3 = -30000$;
 $\alpha_1 = 1.3$; $\alpha_2 = 5$; $\alpha_3 = -2$;

Details of input loading

The isolator is subjected to a variation of the vertical load to determine the effect of the vertical load on the dynamic properties and the predicting stability of un-bonded isolator under cyclic horizontal displacement. Elastomeric isolator is loaded simultaneously to the design vertical load of 350 kN, which is equal to the axial force in the column of the actual building and two fully reversed sinusoidal cycles of horizontal displacement of amplitude 80 mm ($0.89t_r$) (seen in Fig. 4) applied at the top steel plate. Amplitude of horizontal displacement is increased up to 135 mm ($1.50t_r$). The vertical load is subsequently increased and the process is repeated starting at the displacement amplitude of 80 mm. The complete simulation is considered for three displacement amplitudes of 80, 112.5 and 135 mm ($0.89t_r$, $1.25t_r$ and $1.50t_r$) and four vertical loads of 350, 550, 700 and 850 kN. In addition, the horizontal response of the un-bonded isolator is also conducted under the design vertical load of 350 kN and increasing horizontal displacement up to $2.00t_r$ (180 mm) to investigate the rollout instability.

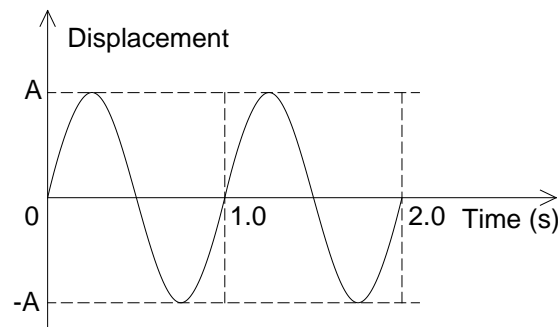
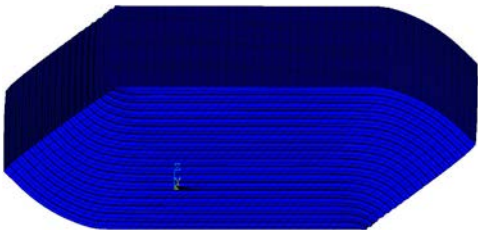


Fig. 4. Imposed horizontal displacement history versus time

Finite element model validation

For the finite element model validation, the numerical results are compared with experimental findings from test conducted at the structural laboratory in IIT Guwahati, India for a prototype un-bonded isolator. This specimen with the same size, component layers and material properties as given in Table 1 is checked here before using in an actual building in Tawang, India. In this test, the specimen is subjected simultaneously to a constant vertical load of 350 kN and three fully reversed sinusoidal cycles of horizontal displacement of amplitude 20 mm

($0.22t_r$), 40 mm ($0.44t_r$), 60 mm ($0.67t_r$) and 80 mm ($0.89t_r$). Comparisons of numerical and experimental results are conducted to evaluate the accuracy of FE model.



a) Deformed shape from numerical simulation



b) Deformed shape from experiment

Fig. 5. Deformed shapes of an un-bonded isolator at displacement amplitude of 80 mm

Deformed shapes of isolator as obtained from both numerical and experimental result at the horizontal displacement amplitude of 80 mm are shown in Fig. 5. The top and bottom surfaces of un-bonded FREI exhibit stable roll off the contact surfaces without any damage and resulting in development of very low tensile stresses in that zone. This leads to reduction of the effective horizontal stiffness of the isolator. It can be seen from this Fig.5 that the deformed shapes of the isolator from FE analysis are observed to be in very good agreement with that from experimental test.

Fig. 6 shows the back bone curve for horizontal load-displacement relationships of the un-bonded isolator for displacement up to $0.89t_r$ (80 mm) as obtained from both experiment and FE analysis. Good agreement is observed between the experimental and FE analysis results. It can be seen from the figure, the horizontal load-displacement relation is nearly linear in the range of small displacement. Slope of this line is the effective horizontal stiffness of the isolator. When displacement increases, the response of un-bonded isolator becomes nonlinear due to the rollover. Consequently, the horizontal stiffness decreases with the increasing horizontal displacement. Fundamental period of un-bonded isolator thus increases with the decrease in stiffness, which result in increasing seismic mitigation capacity of isolator.

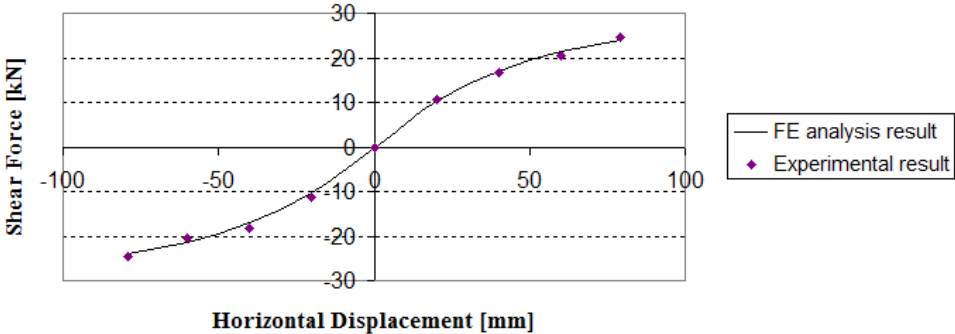


Fig. 6. Horizontal load versus displacement of the un-bonded FREI

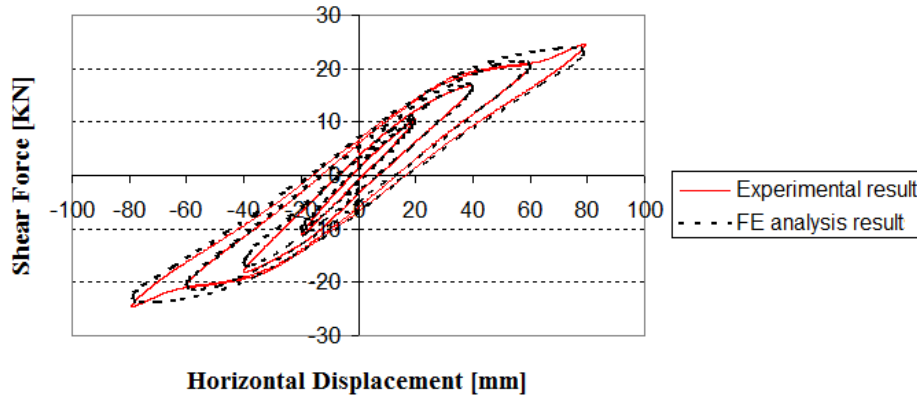


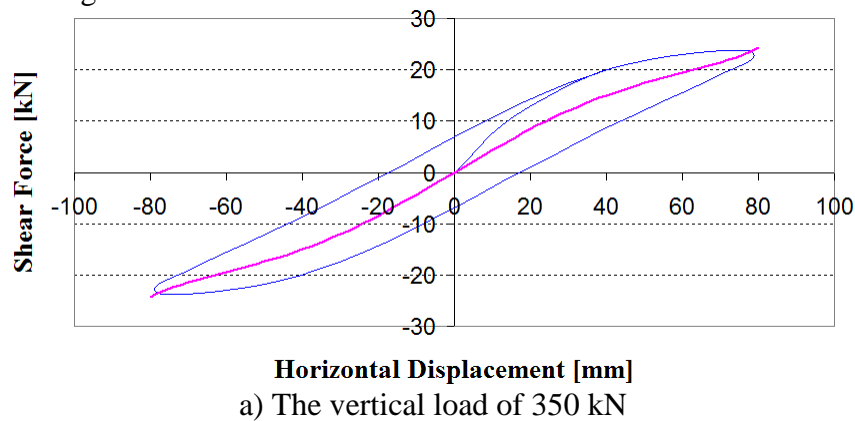
Fig. 7. Comparison of hysteresis loops for the un-bonded isolator by FEA and experimental results

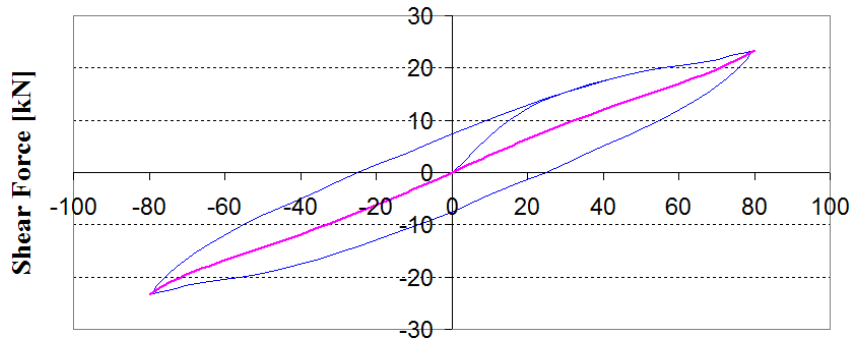
Comparison of the hysteresis loops of the un-bonded isolator obtained as from experiment and FE analysis is presented in Fig. 7, which shows the discrepancy to be quite less. Thus, the adopted finite element analysis strategy is really effective in evaluating the dynamic response of un-bonded FREI under cyclic loading.

Finite element analysis and discussion

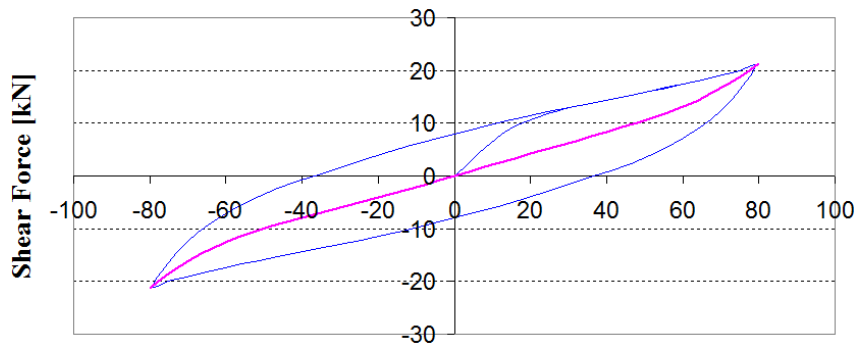
Critical buckling load capacity

The objective of the dynamic stability analysis is to determine the critical buckling load at which the tangential stiffness becomes zero or the isolator would no longer be able to maintain positive incremental force resisting capacity. As noted above, the isolator is subjected to a variation of the vertical loads under cyclic horizontal displacement. According to the fitting method, the fitted backbone curves and corresponding hysteresis loops of the un-bonded isolator for each vertical load and displacement amplitude up to 80 mm as obtained from FE analysis are shown in Fig. 8. The fitted backbone curve is obtained from the average value of shear forces at any given horizontal displacements in the corresponding hysteresis loop and described by a polynomial. It can be seen from the figure, each cycle of FE analysis result maintains both symmetric and comparable hysteresis loops for all the vertical loads investigated. Similarly, considering other displacement amplitudes ($1.25t_r$ and $1.50t_r$), the fitted backbone curves of the isolator under different vertical loads (350, 550, 700 and 850 kN) are shown in Fig. 9.

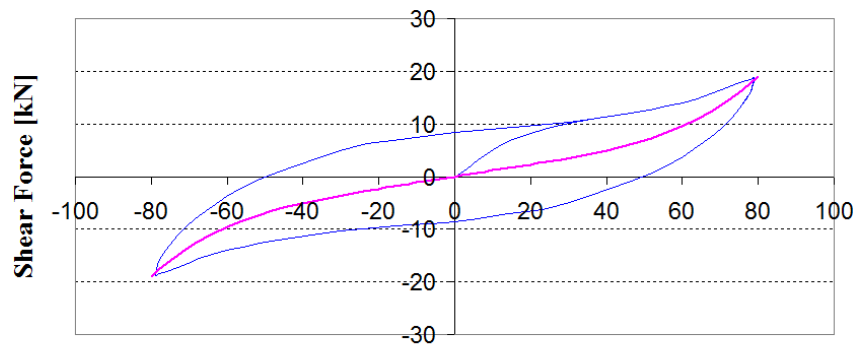




Horizontal Displacement [mm]
b) The vertical load of 550 kN

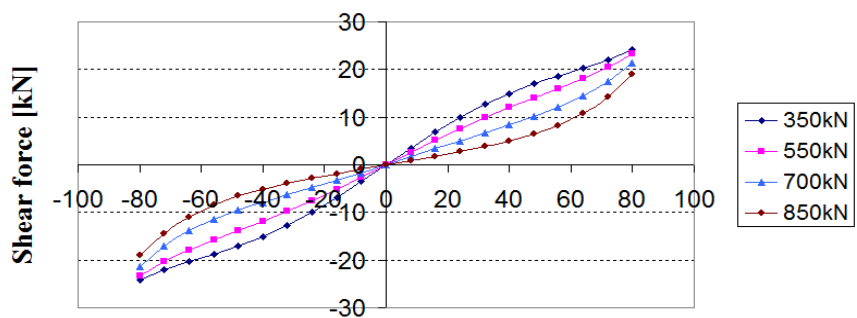


Horizontal Displacement [mm]
c) The vertical load of 700 kN



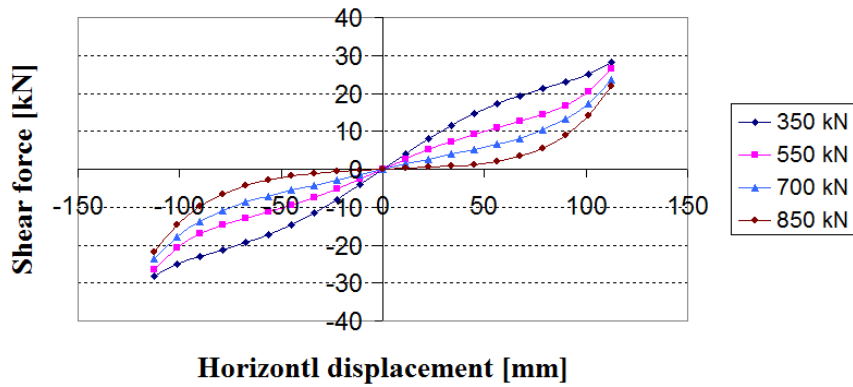
Horizontal Displacement [mm]
d) The vertical load of 850 kN

Fig. 8. Hysteresis loops with backbone curves of the isolator at displacement amplitude of 80 mm

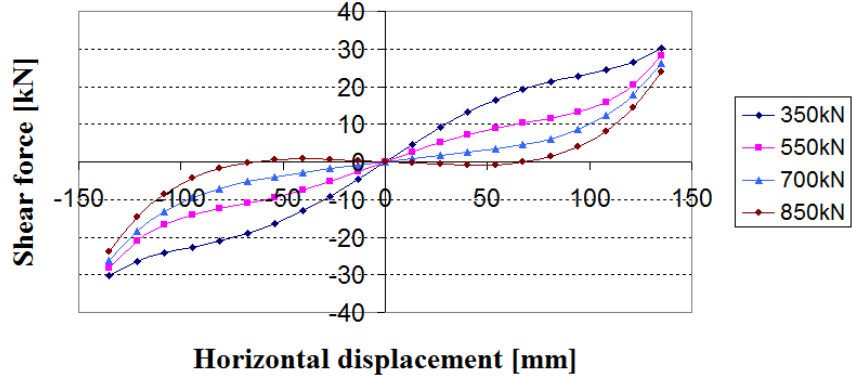


Horizontal displacement [mm]

a) Displacement amplitude of $0.89t_r$ (80 mm)

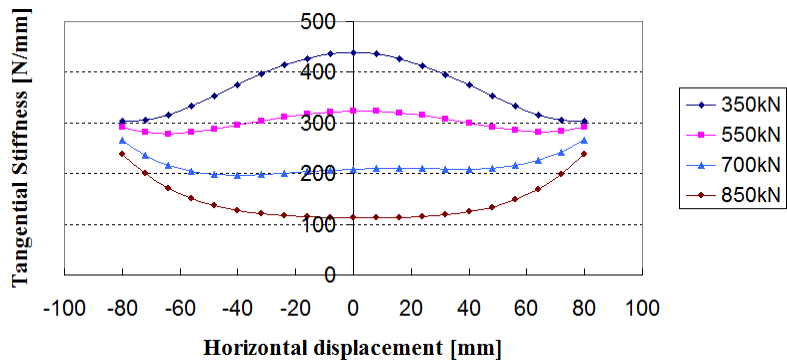


b) Displacement amplitude of $1.25t_r$ (112.5 mm)

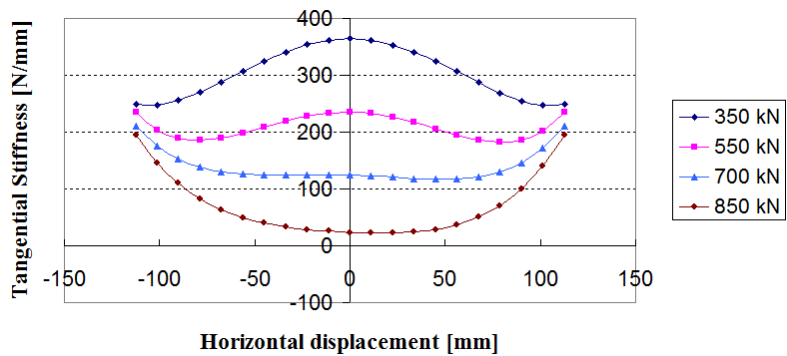


c) Displacement amplitude of $1.50t_r$ (135 mm)

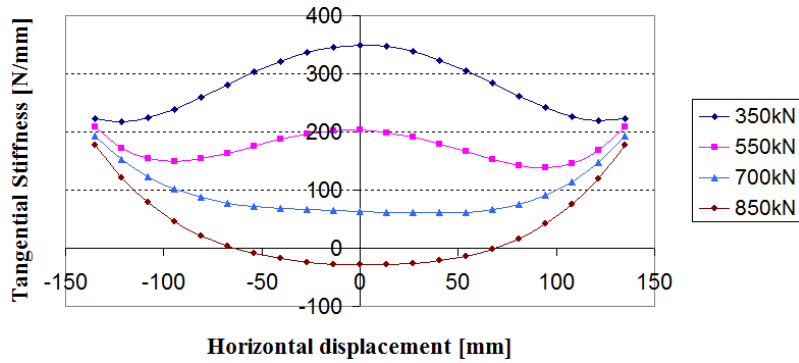
Fig. 9. Fitted backbone curves of the un-bonded isolator at the horizontal displacement amplitudes of $0.89t_r$, $1.25t_r$ and $1.50t_r$



a) Displacement amplitude of $0.89t_r$ (80 mm)



b) Displacement amplitude of $1.25t_r$ (112.5 mm)



c) Displacement amplitude of $1.50t_r$ (135 mm)

Fig. 10. Tangential stiffness obtained from the first derivative of the fitted backbone curve at the horizontal displacement amplitudes of $0.89t_r$, $1.25t_r$ and $1.50t_r$

The values of tangential stiffness results are evaluated from Eq. (11) and are presented in Fig. 10. The tangential stiffness at zero horizontal displacement, does not represent the minimum effective stiffness in a fully reversed sinusoidal cycle of horizontal displacement under low vertical loads of 350 and 550 kN. As the vertical load increases, the minimum slope of the backbone curve (tangential stiffness) occurs at zero horizontal displacement. At the large horizontal displacement and under large vertical loads, the transverse stiffness may acquire a negative value (Fig. 10c). Consequently, the vertical load corresponding to zero transverse stiffness is predicted by the approximation method.

As discussed above, the vertical load corresponding to zero transverse stiffness is defined as the critical buckling load for an un-bonded FREI. The points corresponding to zero transverse stiffness of the un-bonded isolator for different amplitudes of horizontal displacement as obtained by approximation method are shown in Fig. 11. As expected, the transverse stiffness decreases with the increase of the vertical load. The critical buckling loads are obtained from the points which have zero transverse stiffness. The relation of these critical buckling loads versus the horizontal displacement amplitude is shown in Fig. 12.

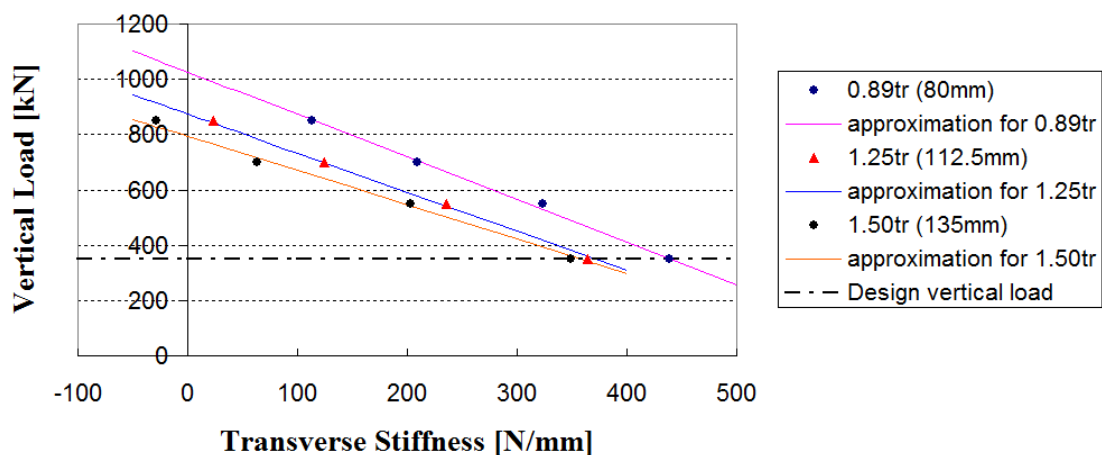


Fig. 11. Influence of the vertical load on transverse stiffness for the un-bonded isolator

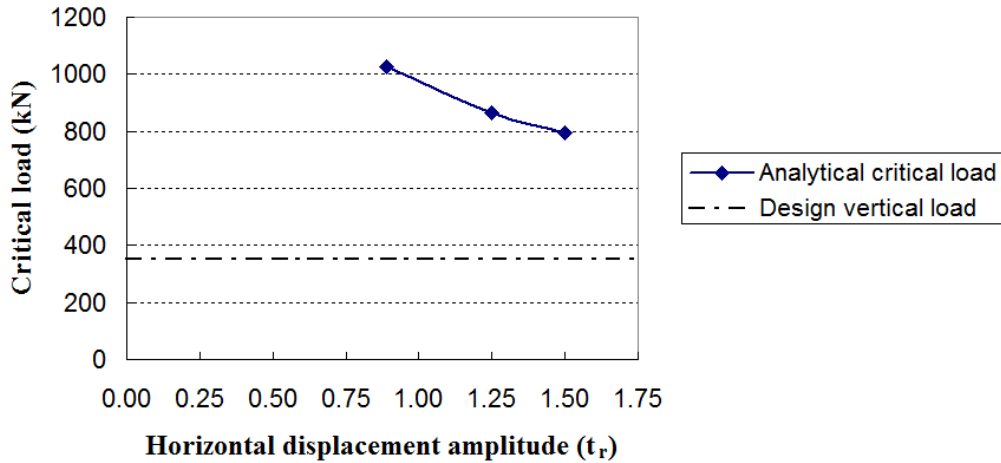


Fig. 12. The critical buckling load capacity of the un-bonded FREI.

It can be seen from the Fig. 12 that the critical buckling load decreases with the increase of the horizontal displacement amplitude, and it is relatively great at low displacement amplitude. The critical load capacity as obtained from FE analysis is significantly higher than the design vertical load, as example, the critical loads are found to be 2.9, 2.5 and 2.3 times higher than the design vertical load at displacement amplitude of $u = 0.89t_r$, $1.25t_r$ and $1.50t_r$, respectively. It is similar to the observation made by Raaf, et al. [2011] based on the experimental critical load carrying capacity of a scaled un-bonded isolator. From these results, it is thus realized that the prototype un-bonded specimen in the experimental tests didn't obviously show any sign of damage and susceptibility to buckling under the design vertical load.

The influence of vertical load on dynamic properties of the isolator

During the course of evaluation of critical load carrying capacity of the isolator, the effect of the vertical loads on the characteristic properties of the un-bonded isolator under cyclic horizontal displacement is also investigated. The effective horizontal stiffness and damping factor of the isolator under the variation of the vertical loads and amplitudes of displacement obtained from equation (4) and (5) are provided in Table 2 and plotted in Fig. 13.

Table 2. Characteristic properties of un-bonded isolator

Vertical load (kN)	Amplitude of horizontal displacement					
	0.89 t_r (80mm)		1.25 t_r (112.5mm)		1.50 t_r (135mm)	
	K_{eff}^h (kN/m)	β (%)	K_{eff}^h (kN/m)	β (%)	K_{eff}^h (kN/m)	β (%)
350	301.67	13.46	247.09	14.58	222.03	15.42
550	288.09	15.61	233.67	16.92	209.04	17.87
700	267.53	18.19	218.00	19.90	189.40	21.04
850	238.72	21.69	194.13	24.45	165.19	27.00

It can be seen from Fig. 13 that the effective horizontal stiffness of the un-bonded isolator decreases, while the equivalent viscous damping increases with the increase in the vertical load at a given amplitude of horizontal displacement. The decreases of the effective stiffness are found to be 20.9%, 21.4% and 25.6% under the vertical load ranging from 350 kN to 850

kN at the displacement amplitudes of $0.89t_r$, $1.25t_r$ and $1.50t_r$, respectively. At a given vertical load, the effective horizontal stiffness decreases and the damping factor increases with the increasing horizontal displacement amplitudes. It is presented in more detail later. Despite the reduction in the effective horizontal stiffness at high vertical loads, the un-bonded isolator could maintain symmetric force-displacement hysteresis under cyclic loading.

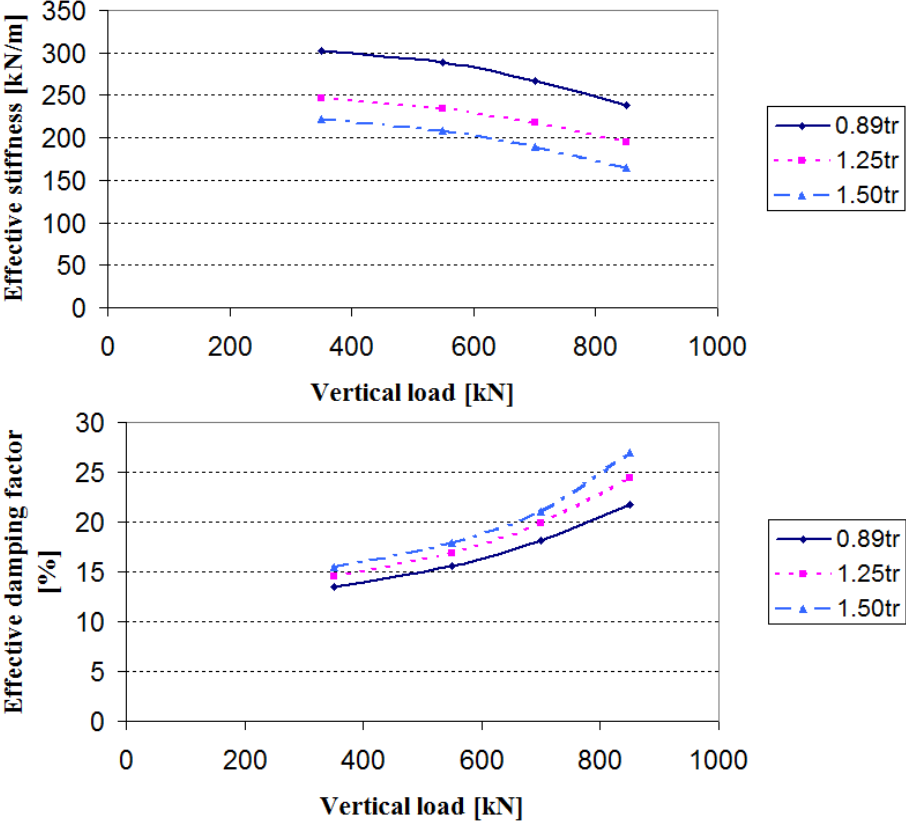


Fig. 13. The relation of the effective horizontal stiffness and damping factor versus vertical load

The rollout instability of the un-bonded FREI under design vertical load

As observed, the un-bonded isolator is not susceptible to buckling under the design vertical load at the amplitude of displacement less than $1.50t_r$. In this case, it is necessary to investigate the horizontal response of the un-bonded isolator under design vertical load of 350 kN and increasing horizontal displacement such that the original vertical faces of isolator establish full contact with the support surfaces, herein up to $2.00t_r$ (180 mm). At the large horizontal displacement, rollover deformation of the un-bonded isolator occurs and the rollout instability may be observed. Rollover is defined as the instability of a recessed isolator under shear displacement. The objective is to determine the horizontal displacement amplitude at which the tangential stiffness will be zero under design vertical load.

The shear force-displacement curve and horizontal secant stiffness-displacement relationship of the un-bonded isolator under the design vertical load and increasing horizontal displacement up to $2.00t_r$ are shown in Figs. 14 and 15. It can be seen from these figures that positive force resisting capacity is observed throughout the displacement range between zero to $2.00t_r$, and hence the isolator remains stable. Thus, the rollout instability of the un-bonded isolator is not observed here, although the results provide a shear profile having four stages of the horizontal response of the un-bonded isolator.

As observed in Fig.14, the horizontal stiffness of the un-bonded isolator is nearly linear under small horizontal displacement from zero to a displacement level at which the upper and lower contact surfaces of the isolator start to roll off the supports, denoted by u_r , is at 18 mm ($0.20t_r$). As the horizontal displacement is further increased, rollover deformation is observed in the isolator and the slope of force-displacement curve decrease to induce the reduction in the effective stiffness. At a certain displacement, portions of originally vertical faces of the isolator come in contact with the support surfaces. From these results from FE analysis, at $u = u_c = 1.40t_r$ (126 mm) the appearance of initial contact is observed. More numbers of originally vertical faces make contact with the support surfaces under the additional increase in horizontal displacement. At $u = u_f = 1.88t_r$ (169.2 mm), all the originally vertical faces of the un-bonded isolator are observed to be fully in contact with the supports. When displacement increases from u_r to u_c , the response of shear force-displacement is nonlinear, the effective horizontal stiffness of the isolator decreases due to rollover (seen in Fig. 15). Meanwhile, at the increasing displacement from u_f to $2.00t_r$, the effective stiffness of the isolator increases due to the contact between the originally vertical faces of isolator and the support surfaces. When the displacement changes in u_c to u_f range, the effective horizontal stiffness is affected by two things: a reduction due to rollover deformation and an increase due to the contact between the originally vertical faces of isolator and the support surfaces. Thus, there exists a transition point in the range of u_c and u_f in which the increase in the effective horizontal stiffness of the isolator due to contact exceeds the decrease in the stiffness due to rollover, and here a hardening behaviour is observed at displacement $u_h = 1.70t_r$ (153 mm). As seen from Fig. 15, the horizontal stiffness get the minimum value at the hardening point. At larger horizontal displacement $u > 2.00t_r$, the increase in horizontal stiffness is very less and the deformed shape of the isolator maintains full contact between the originally vertical faces of the isolator and the supports. The horizontal stiffness of the isolator is found to increase by approximately 32% as the horizontal displacement increases from u_h to $2.00t_r$. This hardening behaviour is advantageous as it can limit the horizontal displacement of the isolation system when subjected to extreme horizontal excitation events. The deformed shapes of the un-bonded isolator at different horizontal displacements as obtained from FE analysis results are shown in Fig. 16.

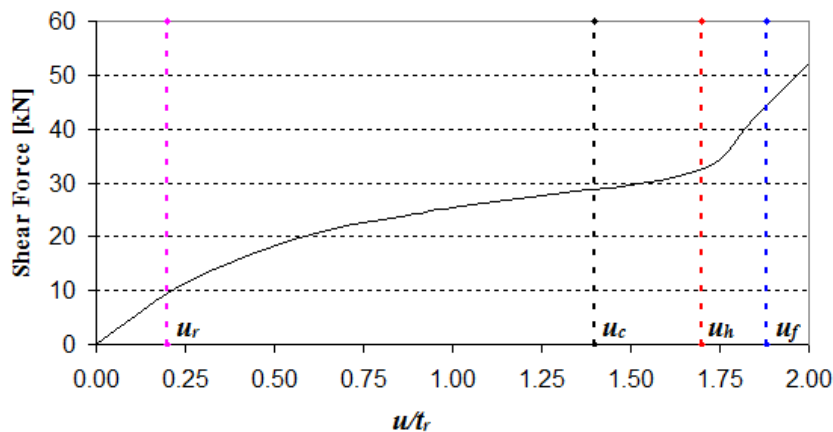


Fig. 14. Horizontal load–displacement curve of the un-bonded isolator.

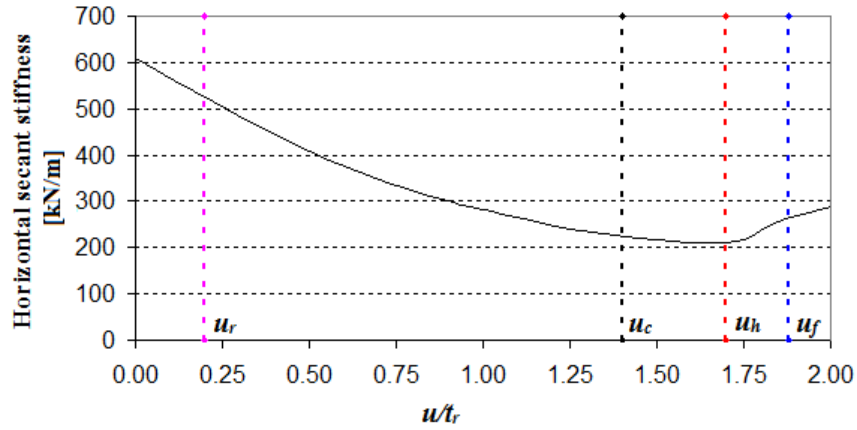


Fig. 15. Horizontal secant stiffness versus displacement

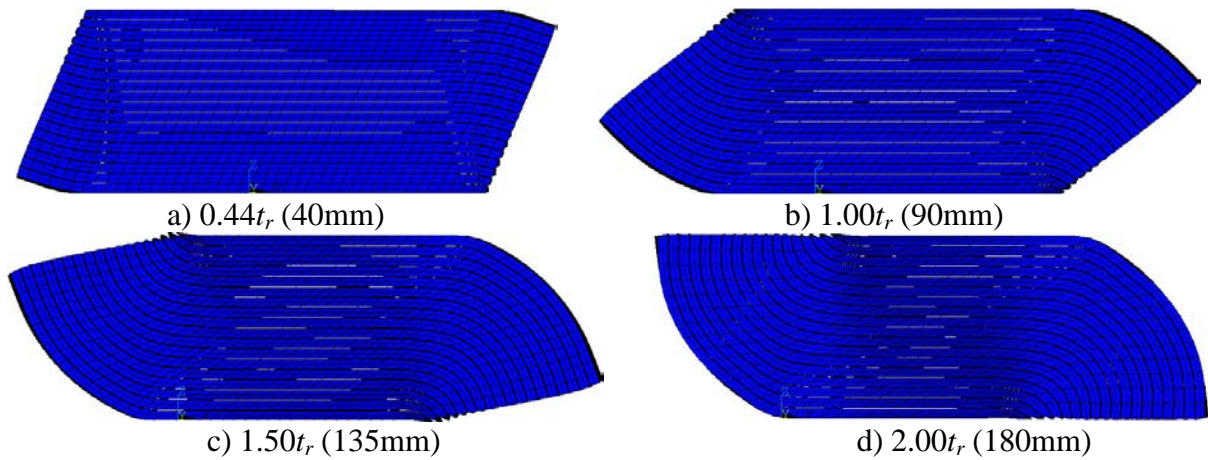


Fig. 16. Deformed shapes of un-bonded isolator obtained from FE analysis results

Conclusions

This paper presents the prediction of stability of a prototype un-bonded fibre-reinforced elastomeric isolator based on response from finite element analysis. The prototype isolators with the same dimensions, component layers and material properties are in use in an actual building in Tawang, India. Size of the isolator is 250 x 250 x 100 mm with the shape factor of 12.5 and aspect ratio of 2.50. In this study, the isolator is subjected to a variation of the vertical loads under cyclic horizontal displacement to determine the effect of the vertical load on the dynamic properties and the predicting stability of the isolator in an un-bonded application. In addition, the horizontal response of the isolator is also gradually increased to investigate the rollout instability under the design vertical load. The concluding remarks are as follows.

- The critical buckling load of the isolator as obtained by dynamic stability analysis corresponds to the point in which tangential stiffness is reduced to zero. The critical buckling load of the isolator decreases with the increase of the horizontal displacement amplitude.
- The critical load carrying capacity of the prototype isolator as obtained from FE analysis is significantly higher than the design vertical load. The critical loads are found to be 2.9, 2.5 and 2.3 times higher than the design vertical load at displacement amplitude of $u = 0.89t_r$, $1.25t_r$ and $1.50t_r$ respectively. It establishes the observation that the actual isolator in experimental testes didn't show any sign of damage and susceptibility to buckling under the design vertical load.

- The effective horizontal stiffness of the un-bonded isolator decreases, while the damping factor increases with the increase in the vertical load at a given amplitude of horizontal displacement.
- The effective horizontal stiffness of the un-bonded isolator decreases, while the damping factor increases with the increase in amplitude of horizontal displacement at a given value of applied vertical load.
- In the behaviour of the isolator under design vertical load, the effective horizontal stiffness decreases at the increasing horizontal displacement. However, under larger displacement up to $2.00t_r$, the horizontal stiffness starts to increase due to the contact between the vertical faces of the isolator with the support surfaces.

Acknowledgements

These authors would like to acknowledge the contribution of METCO Pvt. Ltd., Kolkata, India, for manufacturing FREI and Structural Engng. Laboratory, IIT Guwahati, India for extending facility for experimental investigation.

References

- [1] Buckle I.G., Kelly J.M. [1986], "Properties of Slender Elastomeric Isolation Bearings During Shake Table Studies of a Large-Scale Model Bridge Deck", *Joint Sealing and bearing systems for concrete structures*, ACI, Detroit, Mich., Vol. 1, pp. 247–269.
- [2] Buckle I.G., Liu H. [1993], "Stability of elastomeric seismic isolation systems", *Proc. Sem. Seismic Isolation, Passive Energy Dissipation and Active Control*, Applied Technology Council, Report ATC17-1, pp. 293-305.
- [3] Buckle I.G., Liu H. [1994], "Experimental Determination of Critical Loads of Elastomeric Isolators at High Shear Strain", *NCEER Bulletin*, Vol. 8(3), pp. 1-5.
- [4] Buckle I., Nagarajaiah S., Ferrell K. [2002], "Stability of Elastomeric Isolation Bearings: Experimental study", *Journal of Structural Engineering, ASCE*, Vol. 128(1), pp. 3-11.
- [5] Han X., Kelleher C.A., Warn G.P., Wagener T. [2013], "Identification of the Controlling Mechanism for Predicting Critical Loads in Elastomeric Bearings", *Journal of Structural Engineering, ASCE*, Vol. 139(12), 04013016.
- [6] Haringx J.A. [1948], "One highly compressible helical springs and rubber rods and their application for vibration-free mountings. I.", *Philips Res. Rep.*, Vol. 3, pp. 401-449.
- [7] Haringx J.A. [1949a], "One highly compressible helical springs and rubber rods and their application for vibration-free mountings. II.", *Philips Res. Rep.*, Vol. 4, pp. 49-80.
- [8] Haringx J.A. [1949b], "One highly compressible helical springs and rubber rods and their application for vibration-free mountings. III.", *Philips Res. Rep.*, Vol. 4, pp. 206-220.
- [9] Holzapfel G.A. [1996], "On large strain viscoelasticity: Continuum formulation and finite element applications to elastomeric structures", *International Journal for Numerical Methods in Engineering*, Vol. 39, pp. 3903-3926.
- [10] Iizuka M. [2000], "A macroscopic model for predicting large-deformation behaviours of laminated rubber bearings", *Engineering Structures, ELSEVIER*, Vol. 22(4), pp. 323-334.
- [11] Kelly J.M. [1999], "Analysis of Fibre-Reinforced Elastomeric Isolators", *Earthquake Engineering Research Center, University of California, Berkeley, USA, JSEE*, Vol. 2(1), pp. 19-34.
- [12] Kelly J.M., Konstantinidis D.A. [2011], "Mechanics of Rubber Bearings for Seismic and Vibration Isolation", *John Wiley & Sons, Ltd*, Publication.
- [13] Kelly J.M., Calabrese A. [2012], "Mechanics of Fibre Reinforced Bearings", *PEER Report*, 2012/101, Pacific Earthquake Engineering Research Center, University of California, Berkeley, USA.
- [14] Koh C.G., Kelly J.M. [1989], "Viscoelastic Stability Model for Elastomeric Isolation Bearings", *Journal of Structural Engineering, ASCE*, Vol. 115(2), pp. 285-302.
- [15] Nagarajaiah S., Ferrell K. [1999], "Stability of Elastomeric Seismic Isolation Bearings", *Journal of Structural Engineering, ASCE*, Vol. 125(9), pp. 946-954.
- [16] Osgoee P.M., Tait M.J., Konstantinidis D. [2014], "Finite element analysis of unbonded square fibre-reinforced elastomeric isolators (FREIs) under lateral loading in different directions", *Composite Structures, ELSEVIER*, Vol. 113, pp. 164-173.
- [17] Raaf M.G.P.D., Tait M.J., Toopchi-Nezhad H. [2011], "Stability of Fibre-reinforced Bearings in an Unbonded Application", *Journal of Composite Materials, SAGE*, Vol. 45(18), pp. 1873-1884.

- [18] Sanchez J., Masroor A., Mosqueda G., Ryan K. [2013], "Static and Dynamic Stability of Elastomeric Bearings for Seismic Protection of Structures", *Journal of Structural Engineering, ASCE*, Vol. 139(7), pp. 1149-1159.
- [19] Southwell, R.V. [1932], "On the analysis of experimental observations in problems of elastomer stability", *Proc. R. Soc. Lond. A*, Vol. 135(828), pp. 601-616.
- [20] Stanton J.F., Scroggins G., Taylor A.W., Roeder C.W. [1990], "Stability of Laminated Elastomeric Bearings", *Journal of Engineering Mechanics, ASCE*, Vol. 116(6), pp. 1351-1371.
- [21] Toopchi-Nezhad H., Tait M.J., Drysdale R.G. [2008a], "Testing and Modelling of Square Carbon Fibre-reinforced Elastomeric Seismic Isolators", *Structural Control and Health Monitoring*, Vol. 15, pp. 876-900.
- [22] Toopchi-Nezhad H., Tait M.J., Drysdale R.G. [2008b], "A Novel Elastomeric Base Isolation System For Seismic Mitigation of Low-rise Buildings", *Proceedings of the 14th World Conference on Earthquake Engineering, October 12-17, Beijing, China*.
- [23] Toopchi-Nezhad H., Drysdale R.G., Tait M.J. [2009a], "Parametric Study on the Response of Stable Unbonded-Fibre Reinforced Elastomeric Isolator (SU-FREIs)", *Journal of Composite Materials, SAGE*, Vol. 43(15), pp. 1569-1587.
- [24] Toopchi-Nezhad H., Tait M.J., Drysdale R.G. [2009b], "Simplified Analysis of a Low-rise Building Seismically Isolated with Stable Un-bonded Fibre Reinforced Elastomeric Isolators", *Canadian Journal of Civil Engineering*, Vol. 36(7), pp. 1182-1194.
- [25] Toopchi-Nezhad H., Tait M.J., Drysdale R.G. [2011], "Bonded versus Unbonded Strip Fibre Reinforced Elastomeric Isolators: Finite Element Analysis", *Composite structures, ELSEVIER*, Vol. 93, pp. 850-859.
- [26] Vemuru V.S., Nagarajaiah S., Masroor A., Mosqueda G. [2014], "Dynamic Lateral Stability of Elastomeric Seismic Isolation Bearings", *Journal of Structural Engineering, ASCE*, Vol. 140(14), A4014014.
- [27] Weisman J., Warn G.P. [2012], "Stability of Elastomeric and Lead-Rubber Seismic Isolation Bearings", *Journal of Structural Engineering, ASCE*, Vol. 138(2), pp. 215-223.